



¹Laboratório de Modelagem Computacional - LaModel, Instituto de Ciências Exatas - ICEx, Universidade Federal de Alfenas-UNIFAL-MG, Alfenas Minas Gerais, Brasil

²Universidad Nacional Tecnológica del Lima Sur UNTELS, Perú

³Universidad Nacional de la Amazonía Peruana, Iquitos, Perú

⁴Departamento de Farmacobiología, Centro Universitario de Ciencias Exactas e Ingenierías, Universidad de Guadalajara, Guadalajara, Jalisco 44430, México

*Corresponding author: groponp@gmail.com

Received: 01/08/2023/ Last Review: 06/09/2023 Accepted: 18/10/2023

Dynamics and Energetics of a Bromodomain in complex with bromosporine from *Leishmania donovani*

Abstract

Leishmaniasis continues to be a neglected tropical disease, affecting people and animals and causing significant economic losses. Therefore, there is interest in the study and evaluation of new drug targets. In fact, it has been shown that by interfering with lysine-reading proteins such as bromodomain (BMD) there is a decrease in parasite survival. In this study, we researched the dynamics and energetics of the *Leishmania donovani* BMD in complex with bromosporin, which is considered to be a pan-inhibitor of BMDs, with the aim of understanding the molecular recognition mechanism. Molecular dynamics (MD) and non-equilibrium free energy calculation guided by steered molecular dynamics (SMD) simulations showed that the BMD has three flexible amino acid regions and bromosporin exhibiting various recognition states during the interaction. These results corroborate the promiscuity of bromosporin for energetically favourable sites, with the possibility of expanding its inhibition to other bromodomains. Furthermore, these results suggest that Van der Waals interactions have more relevance for complex recognition and residues ASN-87 and TRP-93 are key in forming hydrophobic and H-bond interactions, respectively. This research provides new insights for understanding the recognition mechanism, dynamics and energetics of the complex for the development of new therapeutic strategies.

Keywords: Bromodomain; bromosporine; molecular dynamics; free energy.

Dinámica y Energética de un Bromodominio en complejo con bromosporina de *Leishmania donovani*

Resumen

La leishmaniasis sigue siendo una enfermedad tropical desatendida, que afecta a personas y animales y causa importantes pérdidas económicas. De ahí el interés por estudiar y evaluar nuevas dianas farmacológicas. De hecho, se ha demostrado que al interferir con proteínas lectoras de lisina como el bromodominio ("bromodomain", BMD) se produce una disminución de la supervivencia del parásito. En este artículo estudiamos la dinámica y la energética del BMD de *Leishmania donovani* en complejo con bromosporina, que se considera un pan-inhibidor de BMD, con el objetivo de comprender el mecanismo de reconocimiento molecular. Las simulaciones de dinámica molecular (DM) y el cálculo de energía libre de no-equilibrio guiado por dinámica molecular de estiramiento (DMS) mostraron que BMD tiene tres regiones de aminoácidos flexibles y la bromosporina presenta varios estados de reconocimiento durante la interacción. Estos resultados corroboran la promiscuidad de la bromosporina por sitios energéticamente favorables, siendo posible expandir su inhibición a otros bromodomínios. Además, los resultados sugieren que las interacciones de Van der Waals tienen más relevancia para el reconocimiento del complejo y los residuos ASN-87 y TRP-93 son clave en la formación de interacciones hidrofóbicas y de puentes de hidrógeno, respectivamente. Esta investigación proporciona nuevos conocimientos para comprender el mecanismo de reconocimiento molecular, la dinámica y la energética del complejo para el desarrollo de nuevas estrategias terapéuticas.

Palabras clave: Bromodominio; bromosporina; dinámica molecular; energía libre.

Dinâmica e energética de um bromodomínio em complexo com bromosporina de *Leishmania donovani*

Resumo

A leishmaniose continua a ser uma doença tropical negligenciada, que afeta os seres humanos e os animais e causa perdas econômicas significativas. Daí o interesse em estudar e avaliar novos alvos de medicamentos. De fato, a interferência com proteínas leitoras de lisina, como o bromodomínio ("bromodomain", BMD), tem demonstrado diminuir a sobrevivência do parasita. Neste trabalho, estudamos a dinâmica e a energética do BMD de *Leishmania donovani* em complexo com a bromosporina, considerada um pan-inibidor da BMDs, com o objetivo de compreender o mecanismo de reconhecimento molecular. As simulações de dinâmica molecular (MD) e cálculo de energia livre de não-equilíbrio guiada por dinâmica molecular esticamento (MDS) mostraram que o BMD tem três regiões de aminoácidos flexíveis e que a bromosporina apresenta vários estados de reconhecimento durante a interação. Esses resultados corroboram a promiscuidade da bromosporina para locais energeticamente favoráveis, possibilitando a expansão de sua inibição para outros bromodomínios. Além disso, os resultados sugerem que as interações de Van der Waals são mais relevantes no momento do reconhecimento do complexo e os resíduos ASN-87 e TRP-93 são fundamentais na formação de interações hidrofóbicas e de ligações de hidrogênio, respectivamente. Essa pesquisa fornece novos insights para compreender o mecanismo de reconhecimento, a dinâmica e a energética do complexo para o desenvolvimento de novas estratégias terapêuticas.

Palavras-chave: Bromodomínio; bromosporina; dinâmica molecular; energia livre.



Introduction

Parasitic infections remain one of the most pressing global health concerns of our day, affecting billions of people and producing unsustainable economic burdens [1]-[3]. One of these parasites is *Leishmania*. *Leishmania* are unicellular parasites that cause human and animal illness, considered as a neglected tropical disease, which is transmitted by infected mosquitoes, resulting in a wide range of pathologies [4]-[6]. *Leishmania* (*L.*) *donovani*, is a species of this group of parasites that causes highly virulent fatal visceral leishmaniasis.

Worldwide *L. donovani* is known to cause between 50 000 to 90 000 new cases of kala-azar or visceral leishmaniasis (VL) [7]-[9], with a total of ~0.2 to 0.4 million people in 98 countries. Added to this, the World Health Organisation (WHO) considers leishmaniasis to be prominent among the global causes of death by infectious diseases. Due to the global health problems that this parasite entails, the re-evaluation of new chemotherapeutic treatments is necessary, since it is known that the current ones can fail. It is currently known that antimonials are the first line of treatment against leishmaniasis in many regions of the world [10]-[12].

The recurrent use of antimonials and other pharmacological treatments as a treatment for leishmaniasis, have generated resistance of these parasites to these drugs [13]-[15]. This creates a serious problem, especially in regions where sanitary conditions are poor, and the combination of drugs is not feasible. Therefore, the search for new strategies and targets for drug development becomes an imperative need [16]-[18].

In this regard, it is known that proteins related to transcriptional processes could emerge as excellent targets. A group of proteins known as molecular “readers” of lysine acetylation, containing a bromodomain (BRD) have emerged as key gene expression regulators and a promising new class of drug targets ([1], [19], [20]). The bromodomain was first described in the characterisation of the *Drosophila melanogaster* nuclear remodelling comprised of ~110 amino acids. The bromodomain folds into a left-handed bundle of four α -helices linked by two variable-loop regions (BC and ZA) that form a hydrophobic pocket for the acetylated lysine ([4], [21], [22]).

There is evidence that lysine acetylation is critical in kinetoplastids (*Trypanosoma spp.* and *Leishmania spp.*) [1], [23]-[25]. Therefore, in this research we study the dynamics and energetics of the bromodomain of *L. donovani* in complex with bromosporine, which is considered as a bromodomain pan-inhibitor, with the aim of understanding the mechanism of molecular recognition, and energetics, in order to use this information in future drug development rationally for this group of proteins.

Materials and Methods

System setup

The system was prepared by means of the CHARMM-GUI [26] tool, using the Solution Builder [27] module. Missing atoms in the middle of the bromodomain chain (PDBID: 5C4Q) were added with PDBReader [28], the protein was protonated to pH 7.0 with the PDB2PQR tool [29]. Next, the system was solvated with the TIP3P [30] water model, into a 15 Å cubic box of padding, and a 150 mM concentration of NaCl. Finally, the bromosporine inhibitor was parameterised with the CGenff tool [31]. All simulations were run with NAMD 2.14 [32] and CHARMM36 FF [33] using CGenFF [31] for the ligand only.

MD protocol

The constructed systems were minimised in the presence of a harmonic restraint of 5 kcal mol⁻¹ Å⁻² on the heavy atoms of the ligand and the backbones of the protein for 10 000 steps. Next, the system

was equilibrated in a NVT assembly at a temperature of 300 K for 5 ns, then the system was equilibrated in a second phase in a NpT assembly maintaining a pressure of 1 bar for 10 ns with the same restraint. Finally, production in NpT at 310 K and 1 bar of pressure was performed for 300 ns, for a total of three independent replicates (3 x 300 ns) accumulating a total of 0.9 μ s.

In the equilibration and production steps the Lavengin thermostat and the Nosé-Hoover Langevin piston were used to control temperature and pressure. Atoms of rigid hydrogens were maintained with SETTLE algorithm [34] in waters, while to solute the RATTLE/SHAKE algorithm was used [35]. Short-range, non-bonded and long-range non-bonded interactions were treated with a cut-off scheme at 12 Å and PME [36], respectively. The r-RESPA multiple time step scheme [37] was used in all cases with 2 fs time integration steps.

Non-equilibrium free energy calculation

For this, the system was prepared and equilibrated with the standard protocol of QwikMD [38], with the only exception that a 40 Å extra padding was added into the Z axis to enable pulling. For pulling a potential bias of the form $U^{SMD}(x) = \frac{1}{2}k[vt - (\xi_t - \xi_0)]^2$ was added for the original potential $H^\pm = V^{original} + U^{SMD}$ through the colvars module [39], getting a modified potential (H^\pm). For this, the centre of mass of the ligand ξ_L , was pulling with a speed v of 10 Å ns⁻¹ and k of 7 kcal mol⁻¹ Å⁻² during 4 ns, enough to reach the unbound state. During the pulling the C_α atoms were restrained with a force of 5 kcal mol⁻¹ Å⁻². A total of 20 independent replicates were performed (total 80 ns). The work was computed for numerical integration using $W = v \int_0^{t'} dt' F(t')$.

Based on these simulations, the potential of mean force ($PMF(\xi), \Phi(\xi)$) was reconstructed by means of Jarzynski identity as show in the following equations [40]:

$$\exp[-\beta\Phi(\xi)] = \langle \exp[-\beta W] \rangle_0 \quad (1)$$

If rearranging the equation, it shields the $\Phi(\xi)$:

$$\Phi(\xi) = -\frac{1}{\beta} \log \{ \langle \exp[-\beta W] \rangle \} \quad (2)$$

and expanding this equation for the 2nd order cumulant:

$$\Phi(\xi) = \langle W \rangle - \frac{\beta}{2} [\langle W^2 \rangle - \langle W \rangle^2] + \dots \quad (3)$$

Where $\Phi(\xi)$ is the potential of mean force, i.e the free energy profile over the collective variable (ξ), W is the work done along ξ , and β is the inverse of thermal energy ($1/k_B T$), where k_B is Boltzmann's constant.

On the other hand, to calculate the ΔG_{bind}° standard, we used the following expression:

$$\Delta G_{neq}^{Jarzynski} = \Phi(\xi)^{unbound} - \Phi(\xi)^{bound} \quad (4)$$

then:

$$\Delta G_{bind}^\circ = \Delta G_{neq}^{Jarzynski} + k_B T \ln \left[\frac{C^{comp}}{C^\circ} \right] \quad (5)$$

Where ΔG_{bind}° in kcal mol⁻¹, k_B in kcal mol⁻¹ K⁻¹, $C^{comp} = 1$ ligand Box_{vol}^{-1} is the concentration used in the simulation in Å³ and $C^\circ = 1/1661$ Å³ is the standard concentration yielding 1 ligand \times 1661 Å⁻³. These last two terms are added to pass from the computational system to the standard system. Here $\Phi(\xi)^{bound}$ and $\Phi(\xi)^{unbound}$ correspond to $\Phi(\xi)$ the associated and dissociated thermodynamics state (i.e macrostates) respectively.

Molecular data analysis

All analyses were performed through in-house Tcl/Python scripts based on VMD 1.9.4 [41] and MDAnalysis 2.0 [42], respectively. The images were rendered with VMD 1.9.4 [41]. The plots were generated with R 3.4 [43] and the ggplot [44] library. Interactions throughout the simulations were computed with an in-house python im-

plementation of molecular dynamics interaction plot tool (<https://github.com/tavolivos/Molecular-dynamics-Interaction-plot>).

Results

This work explores the interactions and recognition mechanism of bromosporine in complex with bromodomain. Figure 1 shows the two systems that were constructed, one system (1A) focused on performing conventional molecular dynamics and the second (1B) used to perform the steered molecular dynamics method.

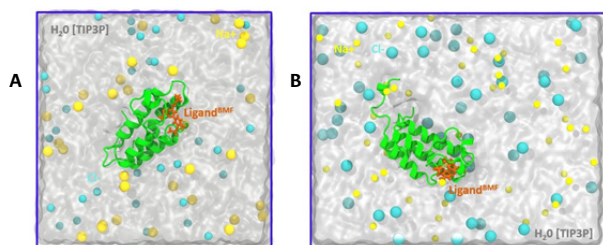


Figure 1. System setup representation **A.** Conventional molecular dynamics representation and **B.** SMD of the bromosporine ligand bound to the bromodomain. All systems contain Na^+ (sky blue) and Cl^- (yellow) ions, while water is represented as the surface in white.

Bromodomain contains flexible regions

In order to evaluate changes in the rigidity/flexibility of the bromodomain structure, root-mean-square fluctuations (RMSF) analyses of the backbone were performed. Protein flexibility and dynamics are essential for the molecular recognition process and play a fundamental role in virtually all biochemical processes in living organisms [45]. The results in Figure 2A show that all the replicates present three flexible regions in the protein and present RMSF values from 1 to 4 Å. Furthermore, Figures 2A, 2B and 2C show the structure of the receptor and the location of the flexible regions. R'_1 ranges from PRO-36 to THR-50, R'_2 from ARG-58 to VAL-72 and finally R'_3 from ASP-85 to ASP-95. The aforementioned flexible regions are structurally composed of loops that play a key role in molecular recognition.

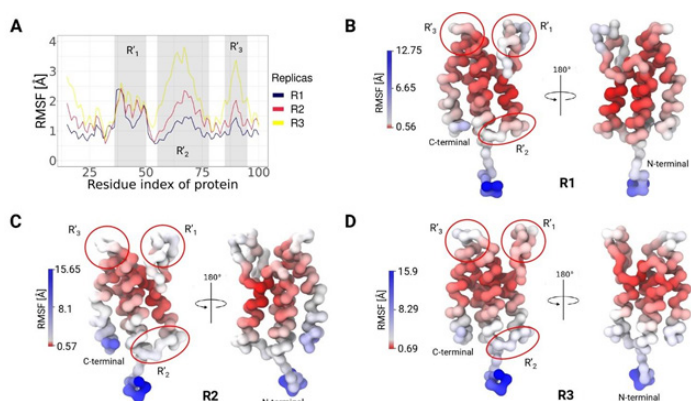


Figure 2. RMSF observed in the bromodomain-bromosporine system by MD. **A.** The bromodomain RMSF is shown except for the terminal regions, where there are three regions of flexibility (R'_1 , R'_2 and R'_3), consistent with the three replicates performed. **B.** **C.** and **D.** highlight the regions of highest flexibility in the bromodomain, excluding the terminal regions. All replicates were presented coloured by β factor on the structure, where red indicates the most stable regions and blue the most fluctuating ones.

Bromosporine presents several recognition states

The stability and structural changes of the bromodomain and bromosporine were evaluated through root-mean-square deviations (RMSD). Figure 3A and 3B indicated different stability values for both; bromodomain presented high values with an average around 5 Å, and bromosporine presented low values 2 Å. The results also indicated that bromosporine presents more than one conformational change. According to the RMSD density plots we noticed three forms of recognition that bromosporine may have in order to interact favourably with the receptor. The obtained RMSD values of the ligand and complex present a correlation because the conformational

changes of the complex, specifically the high plasticity of the pocket, cause freedom of movement of the ligand and could generate several rearrangements during the simulation.

Figures 3D, 3E and 3F using a 2D free energy landscape approach revealed that the ligand scans through three different conformational states had similar results obtained based on the RMSD of the ligand. In addition, based on the RMSD values the 3D structure of the receptor and ligand in the initial structure were obtained, as well as the one showing the maximum RMSD. Both structures were aligned for comparison purposes and to observe the regions showing the highest variability. Figure 3C indicates that the greatest variations in the structure, with respect to the initial one, are in the N-terminal and C-terminal regions.

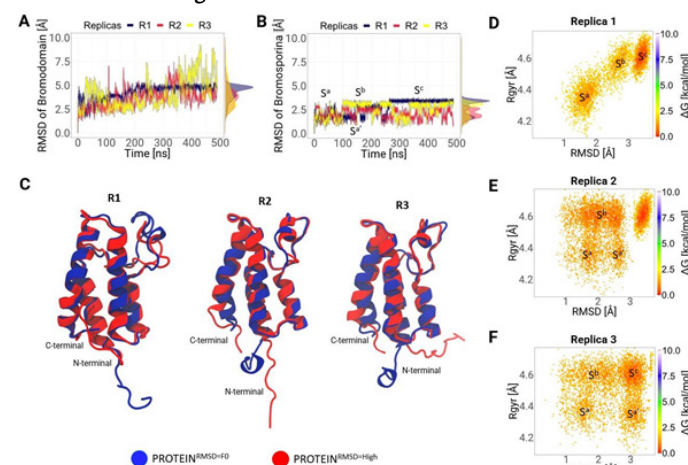


Figure 3. Evolution of the conformational states of the ligand next to the receptor throughout the simulation. **A.** Comparison of the conformational change in the backbone of the bromodomain of the three replicates. **B.** Conformational change of the ligand, where at least three conformational states (S'_a , S'_b and S'_c) were determined. **C.** Structural comparison of the bromodomain at the initial time and at the RMSD max value. **D.** **E.** and **F.** 2D Free energy landscape (FEL) plot of the ligand to the three replicates respectively. All figures contain highlights of the possible conformational states found in the scan.

Pocket

Figure 4 is a set of 3D images showing the bromodomain binding cavity and its associated ligand at three different times. In each image a different conformation of the ligand within the binding cavity is observed. The first image shows the conformation of the ligand at 28 ns with an area of interaction with the receptor determined by the area bounded by the red line. The second image shows a modified conformation of the ligand and the interaction area increases to 193 ns. Finally, the third image shows a new rearrangement of the ligand within the cavity and an increase in the contact area with the receptor. In addition, the images indicate conformational trends of the pocket during the simulation in all replicates, indicating the importance of pocket plasticity.

The relative freedom that can be observed of the ligand during the course of the simulation is due to the constant movement of the loops surrounding the enzyme pocket. The movements allow the ligand to interact with key residues in the complex and start rearranging its atoms until it finds the thermodynamically stable location. The bromosporine at the end of the simulation can fit better because it interacts with the ZA loop which is deeper within the enzyme pocket than the BC loop [46].

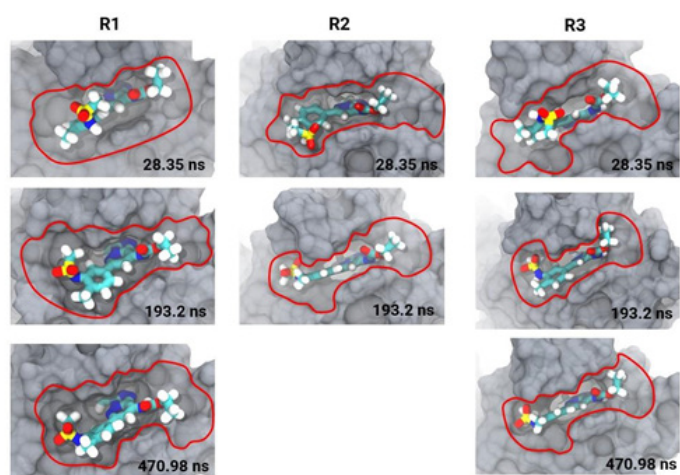


Figure 4. 3D structure of bromosporine in complex with the bromodomain. R1, R2 and R3 present the ligand interaction area in the enzyme pocket, from three replicas, and the conformational states of the ligand at three different times of the simulation.

Van der Waals energy key to molecular recognition

In molecular dynamics simulations, non-bonded energy interactions such as Van der Waals and Coulomb were calculated. Figure 5A and 5B shows the average of the replicas of both energies. Van der Waals interactions contribute more to molecular recognition because they present a strong average energy value of $-40 \text{ kcal mol}^{-1}$ compared to Coulomb interactions with an average weak value of $-27 \text{ kcal mol}^{-1}$. Figure 5C shows a Kruskal-Wallis statistical study performed on both interactions to observe the significant differences between each replicate with a value of $n=5000$. The analyses indicated that there is a significant difference between the replicates in both Van der Waals and Coulomb force.

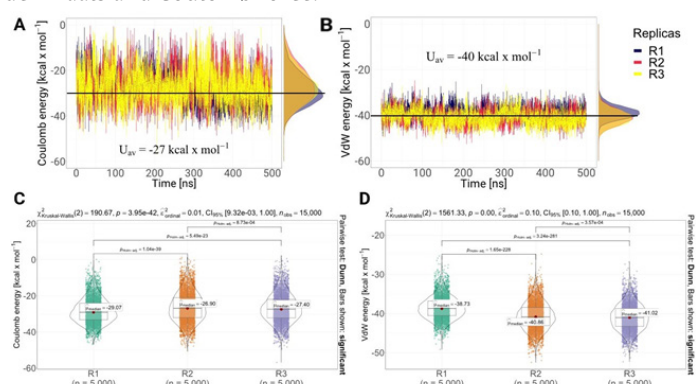


Figure 5. The non-bonded energy of the three replicas shows slight changes (A, B). Kruskal-Wallis statistical test for the C. Electrostatics and D. Van der Waals interaction energies, in which all replicates are statistically different.

Free energy

In Figure 6A, we present the average strength profiles as a function of distance obtained from 20 SMD simulations for the ligand bromosporine bound to the bromodomain complex. At the beginning of each simulation ($t = 0 \text{ ns}$), the ligand is in a bound state, interacting with the protein residues at the binding site. We observe the separation force of the bromosporine bound to the bromodomain complex. In the 20 replicates performed, it is observed that there is a peak of 175 pN near 5 \AA , indicating that there was bond breaking or interactions within the complex. After the peak, near 10 \AA of separation of the complex, the force values drop and do not present any additional energy barrier. In addition, the work of the system was studied. Figure 6B showed a trend in all replicates, where at the beginning of the simulation, the work has an exponential trend up to 25 \AA . After that, the work continues to increase gradually up to 30 \AA and then the system stabilises, causing the work to not increase and generating an asymptote in the replicas. Finally, we calculate the potential of mean force (PMF) using the Jarzynski equation; Figure 6C shows the PMF profiles as a function of stretching distance between the 20 replicates performed along the coordinate set. The

profile consists of two peaks, the first one is near 10 \AA which is the highest value with 60 kcal mol^{-1} and the second one starts after 20 \AA and reaches a value of 40 kcal mol^{-1} at a distance of 25 \AA . The obtained energy ($\Delta G_{\text{bind}}^{\circ}$) value was $43.79 \text{ kcal mol}^{-1}$.

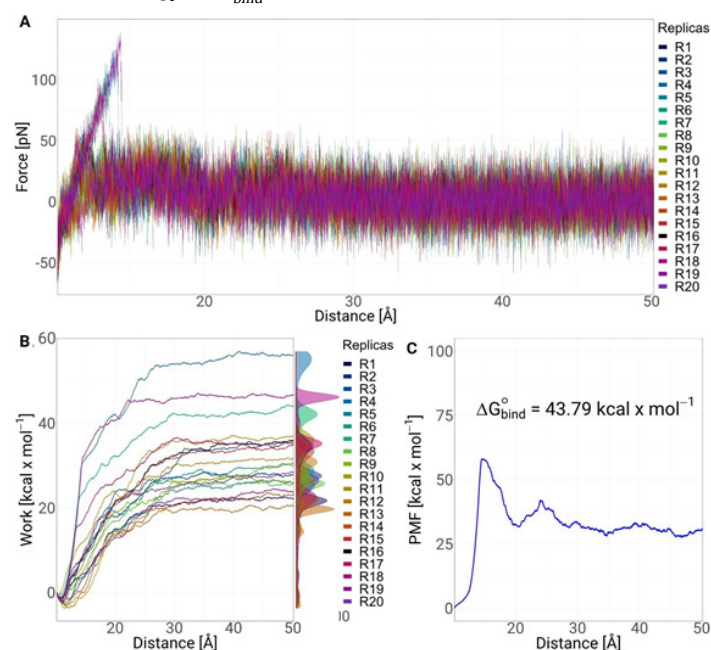
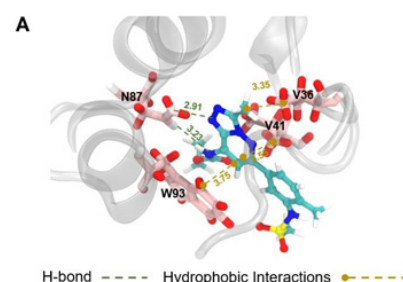


Figure 6. SMD of the bromodomain-bromosporine system. A. Force as a function of distance is shown for the 20 replicates; B. Cumulative system work as a function of distance is shown. C. Potential of mean force (PMF) of the system with respect to the distance is shown.

Asparagine and tryptophan key residues in the binding site

Figure 5A shows 3D images of hydrogen bond interactions and hydrophobic interactions with their respective distances. Key amino acids, especially ASN-87 and TRP-93 interacting with bromosporine and surrounding the hydrophobic bromodomain pocket are observed. In addition, Figures 5B, 5C and 5D show the percentage occurrences of hydrophobic, hydrogen bonding and π -stacking interactions respectively of the bromodomain protein amino acids in the three replicates. Hydrophobic interactions indicated that the amino acid TRP-93 is the one that presented the highest frequency, reaching 20% followed by two Valines at position 36 and 41 that have a similar frequency of 7.5% . On the other hand, in the hydrogen bond the amino acid ASN-87 was the one that clearly presented the highest and most significant values with respect to the remainder of the amino acids. Finally, π -stacking interactions presented the lowest percentage of occurrence with values less than 1% . Both of the aforementioned residues provide the major contribution in the binding of the bromosporine inhibitor to the complex. Therefore, these residues may be effective targets for the development of selective bromodomain inhibitors in *L. donovani*.



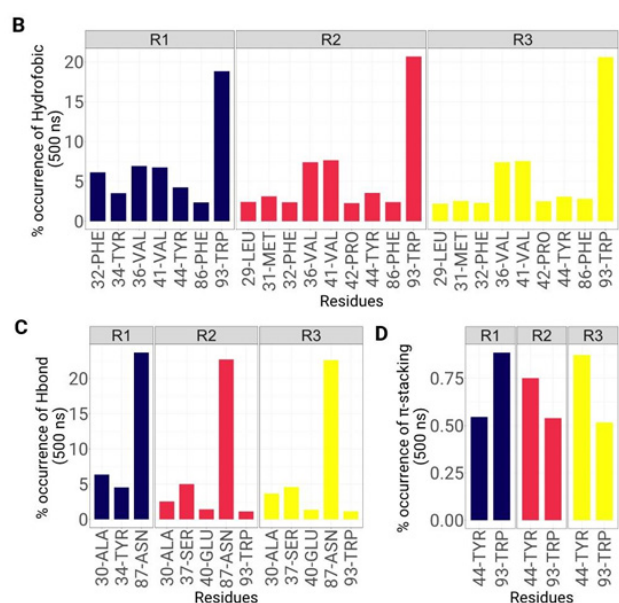


Figure 7. Molecular interactions of the bromosporine-bromodomain system observed during MD. A. The spatial conformation of the system and the key amino acids are shown with the approximate distance in Å, from the crystal structure. B, C, and D show the frequency of occurrence in % of the hydrophobic, H-bond and π -stacking interactions.

Discussion

In this work, we used conventional molecular dynamics and steered molecular dynamics simulations to evaluate the structural dynamics, energetics and recognition mechanism of the bromosporin inhibitor coupled to the bromodomain complex of *L. donovani*.

The analyses showed that in all replicates there are three regions with high fluctuation values. Regions R'_1 and R'_3 correspond to the binding loops; BC and ZA. The values are as expected because both belong to the active site that comes in direct contact with the ligand and it has been shown that the movement of the residues is important for ligand recognition in the bromodomain. The results are similar to those obtained by [47] who analysed eight ligand-coupled bromodomain complexes showing high RMSF values at the active site. The R'_2 region corresponds in the same way to a loop so it is expected to vibrate more with respect to the helix regions [48].

The RMSD values indicated that the replicates obtained from the bromodomain present values > 3.0 Å indicating that they have low stability during the simulation. This may occur due to interaction with the ligand or hydrophobic residues in the loops that may contribute to the instability of the structure [49], [50]. In the case of the ligand results, they showed stability and it could be determined that there are three conformational states. A possible reason for finding multiple states in the ligand is because it is promiscuous and can interact with different structural subfamilies of bromodomains [51]. In fact, it was designed to interact not only with the identified binding site but also with a channel formed by the ZA loop and helix A that is present in almost all bromodomain structures. However, this pocket has rarely been observed to undergo interaction by histone peptide ligands. The observed variations in conformations suggest changes in orientation, position and possible interactions between the ligand and the linker pocket over time. These conformational changes may be essential for the stability and specific interactions between the ligand and the active site. Taken together, the images capture the dynamics of the ligand-cavity complex and provide key information for understanding their interaction at different times in the process [52].

In the case of SMD simulations, the force profiles showed that there is a peak at cleavage of the bromosporin with the bromodomain complex. The observed energy barrier is due to the cleavage

of H-bonds, in this case of ASN-87 with the ligand. Subsequently, the values were observed to drop to zero indicating that the ligand completely dissociates from the binding pocket of the receptor [53], [54]. Similar results were observed in the calculations of work required for uncoupling and PMF which after presenting peaks both started to stabilise after 25 Å [55].

Finally, the binding interaction results between bromodomain and bromosporin indicated that in all three replicates there is H-bond formation of the ASN-87 residue [56]. The data are as expected due to previous investigations, where ligands recognise the central cavity of the receptor and anchor via hydrogen bridging to an asparagine residue present in most bromodomains. In addition, it could be determined that in the BC loop there is TRP-93 which together with VAL-41 and VAL-46 located in the ZA loop are key residues in the hydrophobic interactions allowing the ligand to fully enter the binding site [57], [58].

Conclusion

In this work, we performed computer biomolecular simulations of the bromosporin ligand bound to the bromodomain complex. RMSF and RMSD analyses indicated that the bromodomain has greater flexibility than the ligand, causing the ligand to have freedom of movement and producing three conformational states during the simulation. In addition, it was determined that Van Der Waals interactions are key for the recognition of the ligand to the active site to occur. Finally, it could be determined that residues ASN-87 and TRP-93 surround the enzyme pocket and are located in the BC loop of the complex. Therefore, the findings of this study provide useful dynamic information related to conformational alterations and structure-affinity relationship at atomistic levels for new therapeutic strategies towards the bromodomain.

References

- [1] V. Jeffers, C. Yang, S. Huang, and W. J. Sullivan, "Bromodomains in protozoan parasites: Evolution, function, and opportunities for drug development," *Microbiology and Molecular Biology Reviews*, vol. 81, Mar. 2017, DOI: <https://doi.org/10.1128/mbr.00047-16>.
- [2] C. Tallant *et al.*, "Expanding bromodomain targeting into neglected parasitic diseases," *ACS Infectious Diseases*, vol. 7, no. 11, pp. 2953–2958, 2021, DOI: <https://doi.org/10.1021/acsinfecdis.1c00387>.
- [3] A. Pezza *et al.*, "Essential bromodomain TcBDF2 as a drug target against chagas disease," *ACS Infectious Diseases*, vol. 8, no. 5, pp. 1062–1074, 2022, DOI: <https://doi.org/10.1021/acsinfecdis.2c00057>.
- [4] N. G. Jones *et al.*, "Bromodomain factor 5 is an essential regulator of transcription in leishmania," *Nature Communications*, vol. 13, Dec. 2022, DOI: <https://doi.org/10.1038/s41467-022-31742-1>.
- [5] P. Lypaczewski and G. Matlashewski, "Leishmania donovani hybridisation and introgression in nature: A comparative genomic investigation," *The Lancet Microbe*, vol. 2, pp. e250–e258, Jun. 2021, DOI: [https://doi.org/10.1016/S2666-5247\(21\)00028-8](https://doi.org/10.1016/S2666-5247(21)00028-8).
- [6] P. Grech, S. M. Vella, and T. Piscopo, "Leishmania donovani mucosal leishmaniasis in malta," *BMJ Case Reports*, vol. 13, Nov. 2020, DOI: <https://doi.org/10.1136/bcr-2020-237687>.
- [7] S. Moulik, S. Sengupta, and M. Chatterjee, "Molecular tracking of the leishmania parasite," *Frontiers in Cellular and Infection Microbiology*, vol. 11, Feb. 2021, DOI: <https://doi.org/10.3389/fcimb.2021.623437>.
- [8] E. C. Ashby, J. L. Havens, L. M. Rollosso, J. Hardin, and D. Schulz, "Chemical inhibition of bromodomain proteins in insect-stage African trypanosomes perturbs silencing of the variant surface glycoprotein repertoire and results in widespread changes in the transcriptome," *Microbiology Spectrum*, vol. 11,

- no. 3, pp. e00147–23, 2023, DOI: <https://doi.org/10.1128/spectrum.00147-23>.
- [9] S. A. A. Das Sonali and Mukherjee, “Super enhancer-mediated transcription of miR146a-5p drives M2 polarization during leishmania donovani infection,” *PLoS Pathogens*, vol. 17, no. 2, pp. 1–27, Feb. 2021, DOI: <https://doi.org/10.1371/journal.ppat.1009343>.
- [10] A. Ponte-Sucre *et al.*, “Drug resistance and treatment failure in leishmaniasis: A 21st century challenge,” *PLoS Neglected Tropical Diseases*, vol. 11, Public Library of Science, Dec. 2017, DOI: <https://doi.org/10.1371/journal.pntd.0006052>.
- [11] E. Ashby *et al.*, “Genomic occupancy of the bromodomain protein Bdf3 is dynamic during differentiation of African trypanosomes from bloodstream to procyclic forms,” *mSphere*, vol. 7, no. 3, pp. e00023–22, 2022, DOI: <https://doi.org/10.1128/msphere.00023-22>.
- [12] J. N. Roson *et al.*, “Histone H2B.v demarcates strategic regions in the trypanosoma cruzi genome, associates with a bromodomain factor and affects parasite differentiation and host cell invasion,” *bioRxiv*, 2021, DOI: <https://doi.org/10.1101/2021.06.08.447515>.
- [13] R. García-Hernández, J. I. Manzano, S. Castanys, and F. Gamarró, “Leishmania donovani develops resistance to drug combinations,” *PLoS Neglected Tropical Diseases*, vol. 6, Dec. 2012, DOI: <https://doi.org/10.1371/journal.pntd.0001974>.
- [14] M. A. J. Fleck Krista and Nitz, “‘Reading’ a new chapter in protozoan parasite transcriptional regulation,” *PLoS Pathogens*, vol. 17, no. 12, pp. 1–21, Dec. 2021, DOI: <https://doi.org/10.1371/journal.ppat.1010056>.
- [15] S. Pradhan, R. A. Schwartz, A. Patil, S. Grabbe, and M. Goldust, “Treatment options for leishmaniasis,” *Clinical and Experimental Dermatology*, vol. 47, no. 3, pp. 516–521, Mar. 2022, DOI: <https://doi.org/10.1111/ced.14919>.
- [16] V. Geoghegan, N. G. Jones, A. Dowle, and J. C. Mottram, “Protein kinase signalling at the leishmania kinetochore captured by XL-BioID,” *bioRxiv*, 2021, DOI: <https://doi.org/10.1101/2021.07.08.451598>.
- [17] M. A. A. Jafarzadeh Abdollah and Nemat, “Bidirectional cytokine-microRNA control: A novel immunoregulatory framework in leishmaniasis,” *PLoS Pathogens*, vol. 18, no. 8, pp. 1–17, Aug. 2022, DOI: <https://doi.org/10.1371/journal.ppat.1010696>.
- [18] S. S. Çınaroğlu and E. Timuçin, “Comprehensive evaluation of the MM-GBSA method on bromodomain-inhibitor sets,” *Briefings in Bioinformatics*, vol. 21, no. 6, pp. 2112–2125, Nov. 2019, DOI: <https://doi.org/10.1093/bib/bbz143>.
- [19] A. K. Gupta, S. Das, M. Kamran, S. A. Ejazi, and N. Ali, “The pathogenicity and virulence of leishmania - interplay of virulence factors with host defenses,” *Virulence*, vol. 13, no. 1, pp. 903–935, 2022, DOI: <https://doi.org/10.1080/21505594.2022.2074130>.
- [20] E. Rodriguez Araya, M. L. Merli, P. Cribb, V. C. de Souza, and E. Serra, “Deciphering divergent trypanosomatid nuclear complexes by analyzing interactomic datasets with AlphaFold2 and genetic approaches,” *ACS Infectious Diseases*, vol. 9, no. 6, pp. 1267–1282, 2023, DOI: <https://doi.org/10.1021/acscinfed.3c00148>.
- [21] A. Jafarzadeh *et al.*, “The expression of PD-1 and its ligands increases in leishmania infection and its blockade reduces the parasite burden,” *Cytokine*, vol. 153, p. 155839, 2022, DOI: <https://doi.org/10.1016/j.cyto.2022.155839>.
- [22] S. Zaib and I. Khan, “Synthetic and medicinal chemistry of phthalazines: Recent developments, opportunities and challenges,” *Bioorganic Chemistry*, vol. 105, p. 104425, 2020, DOI: <https://doi.org/10.1016/j.bioorg.2020.104425>.
- [23] C. M. C. Laurin *et al.*, “Fragment-based identification of ligands for bromodomain-containing factor 3 of trypanosoma cruzi,” *ACS Infectious Diseases*, vol. 7, no. 8, pp. 2238–2249, 2021, DOI: <https://doi.org/10.1021/acscinfed.3c00618>.
- [24] J. A. Kavouris *et al.*, “Discovery of pyrazolopyrrolidinones as potent, broad-spectrum inhibitors of leishmania infection,” *Frontiers in Tropical Diseases*, vol. 3, 2023, DOI: <https://doi.org/10.3389/ftd.2022.1011124>.
- [25] S. Khandibharad, K. Kharat, and S. Singh, “Single cell ATAC sequencing identifies sleepy macrophages during reciprocity of cytokines in L.major infection,” *bioRxiv*, 2023, DOI: <https://doi.org/10.1101/2023.01.30.526191>.
- [26] S. Jo, T. Kim, V. G. Iyer, and W. Im, “CHARMM-GUI: A web-based graphical user interface for CHARMM,” *Journal of Computational Chemistry*, vol. 29, no. 11, pp. 1859–1865, 2008, DOI: <https://doi.org/10.1002/jcc.20945>.
- [27] Y. Qi, X. Cheng, W. Han, S. Jo, K. Schulten, and W. Im, “CHARMM-GUI PACE CG builder for solution, micelle, and bilayer coarse-grained simulations,” *Journal of Chemical Information and Modeling*, vol. 54, no. 3, pp. 1003–1009, 2014, DOI: <https://doi.org/10.1021/ci500007n>.
- [28] S. Jo *et al.*, “Chapter eight - CHARMM-GUI PDB manipulator for advanced modeling and simulations of proteins containing nonstandard residues,” in *Biomolecular modelling and simulations*, T. Karabencheva-Christova, Ed., in *Advances in protein chemistry and structural biology*, vol. 96. Academic Press, 2014, pp. 235–265. DOI: <https://doi.org/https://doi.org/10.1016/bs.apcsb.2014.06.002>.
- [29] T. J. Dolinsky, J. E. Nielsen, J. A. McCammon, and N. A. Baker, “PDB2PQR: an automated pipeline for the setup of Poisson-Boltzmann electrostatics calculations,” *Nucleic Acids Research*, vol. 32, no. suppl_2, pp. W665–W667, Jul. 2004, DOI: <https://doi.org/10.1093/nar/gkh381>.
- [30] W. L. Jorgensen, J. Chandrasekhar, J. D. Madura, R. W. Impey, and M. L. Klein, “Comparison of simple potential functions for simulating liquid water,” *The Journal of Chemical Physics*, vol. 79, no. 2, pp. 926–935, Jul. 1983, DOI: <https://doi.org/10.1063/1.445869>.
- [31] K. Vanommeslaeghe and A. D. Jr. MacKerell, “Automation of the CHARMM general force field (CGenFF) i: Bond perception and atom typing,” *Journal of Chemical Information and Modeling*, vol. 52, no. 12, pp. 3144–3154, 2012, DOI: <https://doi.org/10.1021/ci300363c>.
- [32] J. C. Phillips *et al.*, “Scalable molecular dynamics with NAMD,” *Journal of Computational Chemistry*, vol. 26, no. 16, pp. 1781–1802, 2005, DOI: <https://doi.org/10.1002/jcc.20289>.
- [33] Y. Xu, K. Vanommeslaeghe, A. Aleksandrov, A. D. MacKerell Jr., and L. Nilsson, “Additive CHARMM force field for naturally occurring modified ribonucleotides,” *Journal of Computational Chemistry*, vol. 37, no. 10, pp. 896–912, 2016, DOI: <https://doi.org/10.1002/jcc.24307>.
- [34] S. Miyamoto and P. A. Kollman, “SETTLE: An analytical version of the SHAKE and RATTLE algorithm for rigid water models,” *J. Comput. Chem.*, vol. 13, no. 8, pp. 952–962, Oct. 1992, DOI: <https://doi.org/10.1002/jcc.540130805>.
- [35] H. C. Andersen, “Rattle: A ‘velocity’ version of the shake algorithm for molecular dynamics calculations,” *Journal of Computational Physics*, vol. 52, no. 1, pp. 24–34, 1983, DOI: [https://doi.org/10.1016/0021-9991\(83\)90014-1](https://doi.org/10.1016/0021-9991(83)90014-1).
- [36] U. Essmann, L. Perera, M. L. Berkowitz, T. Darden, H. Lee, and L. G. Pedersen, “A smooth particle mesh Ewald method,” *The Journal of Chemical Physics*, vol. 103, no. 19, pp. 8577–8593, Nov. 1995, DOI: <https://doi.org/10.1063/1.470117>.
- [37] M. Tuckerman, B. J. Berne, and G. J. Martyna, “Reversible multiple time scale molecular dynamics,” *The Journal of Chemical Physics*, vol. 97, no. 3, pp. 1990–2001, Aug. 1992, DOI: <https://doi.org/10.1063/1.463137>.
- [38] J. V. Ribeiro *et al.*, “QwikMD - integrative molecular dynamics toolkit for novices and experts,” *Scientific reports*, vol. 6, May 2016, DOI: <https://doi.org/10.1038/srep26536>.
- [39] J. Hénin, L. J. S. Lopes, and G. Fiorin, “Human learning for molecular simulations: The collective variables dashboard in VMD,” *Journal of Chemical Theory and Computation*, vol. 18, no. 3, pp. 1945–1956, 2022, DOI: <https://doi.org/10.1021/acs>.

- jctc.1c01081.
- [40] M. A. Cuendet and O. Michielin, "Protein-protein interaction investigated by steered molecular dynamics: The TCR-PMHC complex," *Biophysical Journal*, vol. 95, no. 8, pp. 3575–3590, 2008, DOI: <https://doi.org/10.1529/biophysj.108.131383>.
- [41] W. Humphrey, A. Dalke, and K. Schulten, "VMD: Visual molecular dynamics," *Journal of Molecular Graphics*, vol. 14, no. 1, pp. 33–38, 1996, DOI: [https://doi.org/10.1016/0263-7855\(96\)00018-5](https://doi.org/10.1016/0263-7855(96)00018-5).
- [42] N. Michaud-Agrawal, E. J. Denning, T. B. Woolf, and O. Beckstein, "MDAnalysis: A toolkit for the analysis of molecular dynamics simulations," *Journal of Computational Chemistry*, vol. 32, no. 10, pp. 2319–2327, 2011, DOI: <https://doi.org/10.1002/jcc.21787>.
- [43] R. Ihaka and R. Gentleman, "R: A language for data analysis and graphics," *Journal of Computational and Graphical Statistics*, vol. 5, no. 3, pp. 299–314, 1996, DOI: <https://doi.org/10.1080/10618600.1996.10474713>.
- [44] P. M. Valero-Mora, "ggplot2: Elegant graphics for data analysis," *Journal of Statistical Software, Book Reviews*, vol. 35, no. 1, pp. 1–3, 2010, DOI: <https://doi.org/10.18637/jss.v035.b01>.
- [45] M. A. Lill, "Efficient incorporation of protein flexibility and dynamics into molecular docking simulations," *Biochemistry*, vol. 50, p. 6157, Jul. 2011, DOI: <https://doi.org/10.1021/B12004558>.
- [46] M. Li et al., "Selective mechanism of inhibitors to two bromodomains of BRD4 revealed by multiple replica molecular dynamics simulations and free energy analyses," *Chinese Journal of Chemical Physics, Online First*, pp. 1–15, Jul. 2022, DOI: <https://doi.org/10.1063/1674-0068/CJCP2208126>.
- [47] S. D. Vita, M. G. Chini, G. Bifulco, and G. Lauro, "Insights into the ligand binding to bromodomain-containing protein 9 (BRD9): A guide to the selection of potential binders by computational methods," *Molecules (Basel, Switzerland)*, vol. 26, Dec. 2021, DOI: <https://doi.org/10.3390/MOLECULES26237192>.
- [48] L. Wang, Y. Wang, Z. Yang, S. Xu, and H. Li, "Binding selectivity of inhibitors toward bromodomains BAZ2A and BAZ2B uncovered by multiple short molecular dynamics simulations and MM-GBSA calculations," *ACS Omega*, vol. 6, pp. 12036–12049, May 2021, DOI: https://doi.org/10.1021/ACSOMEGA.1C00687/ASSET/IMAGES/LARGE/AO1C00687_0008.JPEG.
- [49] P. Filippakopoulos et al., "Histone recognition and large-scale structural analysis of the human bromodomain family," *Cell*, vol. 149, pp. 214–231, Mar. 2012, DOI: <https://doi.org/10.1016/j.cell.2012.02.013>.
- [50] Ran. T et al., "Insight into the key interactions of bromodomain inhibitors based on molecular docking, interaction fingerprinting, molecular dynamics and binding free energy calculation," *Molecular BioSystems*, 2015, DOI: <https://doi.org/10.1039/C4MB00723A>
- [51] S. Picaud et al., "Promiscuous targeting of bromodomains by bromosporine identifies BET proteins as master regulators of primary transcription response in leukemia," *Science Advances*, vol. 2, Oct. 2016, DOI: <https://doi.org/10.1126/SCIADV.1600760>.
- [52] J. Zuber et al., "RNAi screen identifies Brd4 as a therapeutic target in acute myeloid leukaemia," *Nature*, vol. 478, pp. 524–528, Oct. 2011, , DOI: <https://doi.org/10.1038/NATURE10334>.
- [53] J. S. Patel, A. Berteotti, S. Ronsisvalle, W. Rocchia, and A. Cavalli, "Steered molecular dynamics simulations for studying protein-ligand interaction in cyclin-dependent kinase 5," *Journal of Chemical Information and Modeling*, vol. 54, pp. 470–480, Feb. 2014, DOI: https://doi.org/10.1021/CI4003574/SUPPL_FILE/CI4003574_SI_001.PDF.
- [54] N. Martella et al., "Bromodomain and extra-terminal proteins in brain physiology and pathology: BET-ing on epigenetic regulation," *Biomedicines*, vol. 11, p. 750, Mar. 2023, DOI: <https://doi.org/10.3390/BIOMEDICINES11030750>.
- [55] P. C. Do, E. H. Lee, and L. Le, "Steered molecular dynamics simulation in rational drug design," *Journal of Chemical Information and Modeling*, vol. 58, pp. 1473–1482, Aug. 2018, , DOI: https://doi.org/10.1021/ACS.JCIM.8B00261/ASSET/IMAGES/MEDIUM/CI-2018-00261D_0001.GIF.
- [56] D. J. Owen et al., "The structural basis for the recognition of acetylated histone H4 by the bromodomain of histone acetyltransferase gcn5p," *The EMBO journal*, vol. 19, pp. 6141–6149, Nov. 2000, , DOI: <https://doi.org/10.1093/EMBOJ/19.22.6141>.
- [57] S. G. Smith and M. M. Zhou, "The bromodomain: A new target in emerging epigenetic medicine," *ACS chemical biology*, vol. 11, p. 598, Mar. 2016, DOI: <https://doi.org/10.1021/ACS-CHEMBIO.5B00831>.
- [58] J. Meslamani, S. G. Smith, R. Sanchez, and M. M. Zhou, "Structural features and inhibitors of bromodomains," *Drug discovery today. Technologies*, vol. 19, p. 3, Mar. 2016, DOI: <https://doi.org/10.1016/J.DDTEC.2016.09.001>.

Article citation:

G. Ropón-Palacios, M. Chenet-Zuta, J. Ramos-Galarza, A. Gervacio-Villarreal, K. Otazu, R. Cárdenas-Cárdenas, F. Casillas-Muñoz, "Dynamics and Energetics of a Bromodomain in complex with bromosporine from *Leishmania donovani*", *Rev. Colomb. Quim.*, vol. 52, no. 1, pp. 3-9, 2023. DOI: <https://doi.org/10.15446/rev.colomb.quim.v52n1.110374>